

## Heterogeneous Reaction of NO<sub>2</sub> on Fresh and Coated Soot Surfaces

Alexei F. Khalizov, Miguel Cruz-Quinones, and Renyi Zhang\*

Department of Atmospheric Sciences and Department of Chemistry, Texas A&M University, College Station, Texas 77843

Received: March 10, 2010; Revised Manuscript Received: May 10, 2010

The heterogeneous reaction of nitrogen dioxide (NO<sub>2</sub>) on fresh and coated soot surfaces has been investigated to assess its role in night-time formation of nitrous acid (HONO) in the atmosphere. Soot surfaces were prepared by incomplete combustion of propane and kerosene fuels under lean and rich flame conditions and then processed by heating to evaporate semivolatile species or by coating with pyrene, sulfuric acid, or glutaric acid. Uptake kinetics and HONO yield measurements were performed in a low-pressure fast-flow reactor coupled to a chemical ionization mass spectrometer (CIMS), using atmospheric-level NO<sub>2</sub> concentrations. The uptake coefficient and the HONO yield upon interaction of NO<sub>2</sub> with nascent soot depend on the type of fuel and combustion regime and are the highest for samples prepared using fuel rich flame. Heating the nascent soot samples before exposure to NO<sub>2</sub> removes the organic material from the soot backbone, leading to a significant increase in NO<sub>2</sub> uptake coefficient and HONO yield. Continuous exposure to NO<sub>2</sub> reduces the reactivity of soot because of irreversible deactivation of the surface sites. Our results support the oxidation–reduction mechanism involving adsorptive and reactive centers on soot surface where NO<sub>2</sub> is converted to HONO and other products. Coating of the soot surface by different materials to simulate atmospheric aging has a strong impact on its reactivity toward NO<sub>2</sub> and the resulting HONO production. Coating of pyrene has little effect on either reaction rate or HONO yield. Sulfuric acid coating does not alter the uptake coefficient, but significantly reduces the amount of HONO formed. Coating of glutaric acid significantly increases NO<sub>2</sub> uptake coefficient and HONO yield. The results of our study indicate that the reactivity and HONO generating capacity of internally mixed soot aerosol will depend on the chemical composition of the coating material and hence will vary considerably in different polluted environments.

### 1. Introduction

Nitrous acid (HONO), an important night-time reservoir of hydroxyl radical (OH), can be readily photolyzed after dawn, releasing OH into the planetary boundary layer.<sup>1,2</sup> Mixing ratios of HONO up to several parts per billion (ppb) have been observed in urban areas,<sup>3</sup> implicating that HONO plays an important role in O<sub>3</sub> production, particularly shortly after sunrise. A number of mechanisms have been proposed<sup>4</sup> to explain the high night-time concentrations of HONO observed in field measurements.<sup>1</sup> However, model calculations including all known sources, such as gas-phase chemistry, heterogeneous aqueous chemistry of NO<sub>x</sub>, and direct emission from vehicle exhaust could not explain the observed high levels of nitrous acid.

The heterogeneous reaction of NO<sub>2</sub> on soot aerosol leading to the formation of HONO has attracted attention as a possible night-time source of nitrous acid.<sup>5</sup> Soot aerosol, which consists primarily of elemental carbon with variable fraction of organic materials, originates from incomplete combustion of fossil fuels and biomass, with an average emission rate of 8–24 Tg of carbon per year<sup>6</sup> and mass loadings 1.5–20 μg m<sup>-3</sup> in the urban boundary layer.<sup>7</sup> Although carbon soot accounts for less than 10–15% of the total atmospheric aerosol mass, soot particles may provide a significant fraction of available aerosol reaction surface due to their fractal morphology. A recent modeling study has shown that heterogeneous conversion of NO<sub>2</sub> to HONO on soot aerosol surfaces in polluted urban environment can

accelerate the O<sub>3</sub> production in the morning and lead to a notable increase in the daytime O<sub>3</sub> concentration.<sup>8</sup> This study, however, assumed a quantitative conversion of NO<sub>2</sub> to HONO on soot aerosol with a time-independent reaction probability that might have overestimated the contribution from heterogeneously produced HONO to the ozone budget.

Because of its atmospheric relevance, heterogeneous conversion of NO<sub>2</sub> to HONO has been extensively studied in the laboratory for a broad range of NO<sub>2</sub> concentrations on a variety of carbonaceous materials, including commercial black carbon, hydrocarbon flame soot, spark discharge soot, diesel soot, power plant soot, etc.<sup>9–16</sup> Despite the large number of studies, the heterogeneous reaction mechanism leading to HONO formation is not well understood, and significant discrepancies exist in the measured NO<sub>2</sub> kinetic uptake coefficients and HONO yields. Depending on the measurement technique, type of soot, assumed surface area, and initial concentration of NO<sub>2</sub>, the reported uptake coefficients vary over 7 orders of magnitude, from 10<sup>-1</sup> to 10<sup>-8</sup>, and HONO yields vary from a few percent to about 100%. As discussed by Aubin and Abbatt,<sup>16</sup> large uptake coefficients reported in early studies were caused by referencing the kinetic measurements to geometric rather than internal surface areas of samples, whereas low HONO yields might have originated from factors such as different flame combustion conditions and incomplete desorption of HONO from the soot surface in low temperature experiments.

Furthermore, the reactivity of soot can be significantly affected by atmospheric aging through surface oxidation or coating. Most previous studies reported that oxidative aging of the soot surface by O<sub>3</sub> and NO<sub>2</sub> reduces its reactivity and HONO

\* To whom correspondence should be addressed. Phone: 979-845-7656. Fax: 979-862-4466. E-mail: Zhang@ariel.met.tamu.edu.

formation capacity irreversibly.<sup>12,14,16</sup> In a few cases, however, reactivation of soot has been observed after heating<sup>10</sup> or in the presence of water vapor.<sup>17</sup> Treating the soot surface with gaseous nitric acid showed no significant impact on the NO<sub>2</sub> heterogeneous reaction probability or HONO yield for atmospherically relevant HNO<sub>3</sub> concentration levels.<sup>15</sup> For soot coated by sulfuric acid the NO<sub>2</sub> uptake rate was almost independent of the amount of adsorbed H<sub>2</sub>SO<sub>4</sub>, but the HONO yield was reduced to zero for a surface coverage greater than 10<sup>14</sup> H<sub>2</sub>SO<sub>4</sub> cm<sup>-2</sup>.<sup>11</sup> To date, the effect of surface processing on the heterogeneous reaction of soot with NO<sub>2</sub> has been investigated only for a limited number of inorganic species, and either a decrease or no change in the HONO production has been reported. Atmospheric soot is commonly found to be thickly coated by inorganic species<sup>18</sup> and functionalized organic matter,<sup>19</sup> formed from photo-oxidation of hydrocarbons.<sup>20–22</sup> Particularly, low-molecular weight dicarboxylic organic acids represent a significant component of fine particulate matter in the troposphere.<sup>23</sup> However, the effect of organic coatings on soot reactivity toward NO<sub>2</sub> has not yet been investigated.

In the present study, the heterogeneous reaction of hydrocarbon flame soot with atmospheric-level concentration of NO<sub>2</sub> was investigated in a low-pressure, fast-flow reactor coupled to a chemical ionization mass spectrometer (CIMS). Both fresh and coated soot samples were examined to assess the role of soot aerosol internal mixing in the atmosphere on its reactivity and HONO generation capacity. The coated materials included pyrene, sulfuric acid, and glutaric acid, which readily adsorb on soot surface,<sup>24–26</sup> forming coatings that can alter the morphology, hygroscopicity, and optical properties of fractal soot particles.<sup>27–30</sup>

## 2. Experimental Section

**2.1. Soot Sample Preparation and Characterization.** Soot was produced by incomplete combustion of propane and kerosene fuels in a diffusion flame formed by a commercial torch and a kerosene lantern with a glass chimney, respectively. A flame was established by altering the amount of fuel with a valve (propane torch) or by adjusting the length of a wick (kerosene lantern). Soot films were deposited on the inner surface of Pyrex glass tubes (10 cm length and 1.6 cm inner diameter) under rich and lean flame conditions, corresponding to type A and type B samples, respectively.<sup>25</sup> Type A soot films were prepared by allowing the reducing part of flame to touch the soot surface and had a grayish appearance due to the presence of organic matter. It has been reported that “activation” of the soot surface by flame changes its adsorptive behavior toward nitric acid<sup>31</sup> and organic acids<sup>25</sup> and may also be responsible for variability in chemical reactivity of otherwise identical soot samples.<sup>32</sup> During preparation of type B films, the tube was held high above the oxidizing flame tip, resulting in a pitch-black soot surface composed mostly of elemental carbon. Visually uniform soot films were obtained by rotating the sample tube during the coating process, and typical soot sample mass ranged from 1 to 30 mg.

To study the effect of aging on heterogeneous reactivity and HONO yield, soot films were exposed to pyrene, glutaric (pentanedioic) acid, and sulfuric acid vapors in an evacuated glass container with a sample of the coating material placed at the bottom. The bottom part of the container was heated to 85–100 °C, depending on the material, whereas the upper part with the soot-coated tube was kept at room temperature. A 20 sccm (standard cubic centimeters per minute) helium carrier flow was supplied to the bottom of the container through a glass

injector tube to distribute the vapor of the coating material uniformly throughout the soot surface. The coating process was carried out for 30 min for each soot sample. Selected soot samples were exposed to 100% relative humidity (RH) by storing them in a desiccator above pure water. In a few cases, fresh soot samples were treated by *iso*-propanol and toluene to extract polar and nonpolar soluble organic materials, respectively. A soot-coated glass tube was carefully immersed in a graduated cylinder with corresponding solvent and left for several hours. After extraction, adsorbed solvent traces were removed by pumping on the sample in vacuum at room temperature for several hours until no apparent degassing has been observed. Although we did not verify the extraction efficiency directly, NO<sub>2</sub> uptake experiments indicated that the treatment by *iso*-propanol removed enough polar organic material to significantly increase soot reactivity. Neither visual appearance nor integrity of the sample was affected by *iso*-propanol extraction. On the contrary, extraction by toluene, while having no effect on reactivity, often led to partial disintegration of the soot film and its dislodgement from the glass tube surface, indicating that toluene removed nonpolar (e.g., PAH) organic material cementing soot to the glass surface.

Fresh and coated soot samples were examined for the presence of different functional groups and the coating material by attenuated total reflection — fourier transmission spectroscopy (ATR-FTIR). For this purpose, soot samples were collected on aluminum foil that was placed inside the Pyrex sample tubes. After sample collection, the foil was removed from the Pyrex tube and cut into 1 cm wide strips. Each strip was placed, with the soot side downward, onto the surface of a ZnSe crystal (Pike Technologies) of the ATR accessory, and an infrared spectrum was recorded using a Nicolet Magna 560 spectrometer equipped with a liquid nitrogen cooled MCT detector. Typically, 60 scans at a resolution of 4 cm<sup>-1</sup> over a range from 4000 to 600 cm<sup>-1</sup> were averaged to obtain a spectrum. The ATR crystal was cleaned between different samples to avoid cross contamination. A background spectrum with no sample on the face of the crystal was collected before each sample spectrum. An ATR correction was routinely applied to all reported spectra, using an algorithm implemented in the FTIR instrument software.

Internal surface areas of soot samples were characterized from Brunauer, Emmett, and Teller (BET) isotherms<sup>33</sup> measured by Kr adsorption at 77 K, as described in our previous study.<sup>25</sup> An improved constant volume adsorption cell with a vacuum jacket at the top<sup>34,35</sup> was used to hold the samples. Soot samples were degassed at room temperature before BET measurements, unless stated otherwise.

**2.2. Measurements of NO<sub>2</sub> Uptake and HONO Production.** Heterogeneous interaction of NO<sub>2</sub> with soot surfaces was studied in a fast-flow coated-wall reactor coupled to a chemical ionization mass spectrometer (CIMS)<sup>25</sup> as shown in Figure 1. A glass tube with the soot-coated inner surface was inserted into the flow reactor of 30 cm length and 2.0 cm inner diameter, through which a flow of 130 sccm helium carrier gas at a 1.5 Torr total pressure was established, resulting in a 530 cm s<sup>-1</sup> laminar flow. Gaseous NO<sub>2</sub> was introduced to the flow reactor at 1–2 sccm through a movable injector from a glass bulb containing 20–100 ppm NO<sub>2</sub> in He at 800 Torr. The reaction time was varied by changing the injector position relative to that of the soot-coated tube. Uptake of NO<sub>2</sub> and evolution of HONO were monitored by following the signals of NO<sub>2</sub><sup>-</sup> and

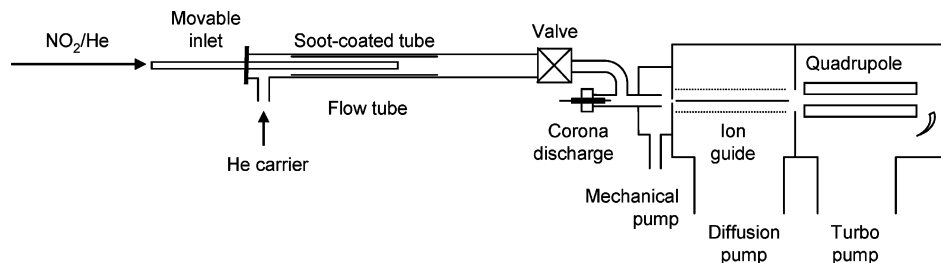


**Figure 1.** Schematic of a low-pressure fast-flow reactor coupled to a chemical ionization mass spectrometer.

$\text{HF} \cdot \text{NO}_2^-$  ions produced in ion–molecule reactions of  $\text{NO}_2$  (eq 1) and HONO (eq 2) with the reagent ion,  $\text{SF}_6^-$ :<sup>36</sup>



Reagent ions were generated by corona discharge in nitrogen carrier gas in the presence of about 10 ppm  $\text{SF}_6$ . Copper and stainless steel tubing and a gas purifier (P-300–2, VICI) were implemented in the CI system to establish an oxygen-free environment (less than 50 ppb  $\text{O}_2$ ) in order to minimize  $\text{NO}_2$  background. Additionally, the CI region of the mass spectrometer was modified to minimize the dissociation of the  $\text{HF} \cdot \text{NO}_2^-$  ion clusters through collisions with bath gas molecules in the electrical field. In several selected experiments  $\text{HF}^- \cdot \text{NO}_3$  ion was monitored to detect formation of  $\text{HNO}_3$  in the reaction of soot with  $\text{NO}_2$ . Concentration of  $\text{NO}_2$  in the flow reactor was  $5 \times 10^9$  to  $5 \times 10^{11}$  molecules  $\text{cm}^{-3}$ , corresponding to mixing ratios of about 0.2–20 ppb at 760 Torr pressure. Previously measured rate coefficients for reaction of  $\text{NO}_2$  with  $\text{SF}_6^-$  and for fluoride ion transfer from  $\text{SF}_6^-$  to HONO are  $1.4 \times 10^{-10}$  and  $6 \times 10^{-10}$   $\text{cm}^3 \text{ molecule}^{-1} \text{ s}^{-1}$ , respectively.<sup>17</sup> Since the latter value is not known with adequate accuracy, additional calibration measurements were performed using two different HONO sources in order to calculate the HONO/ $\text{NO}_2$  concentration ratio from the ratio of their mass spectrometer signals.

In the first method, HONO was synthesized by slowly adding 5 mL of 0.1 M  $\text{NaNO}_2$  to 10 mL of 40 wt %  $\text{H}_2\text{SO}_4$  that was chilled to 273 K and vigorously stirred.<sup>36</sup> During calibration, a flow of about 100 sccm  $\text{N}_2$  was passed through the aqueous HONO solution in a bubbler and then directed into a 11.0 cm long quartz absorption cell located inside a UV/vis Perkin-Elmer spectrophotometer, where optical absorbances at 250 and 450 nm due to  $\text{HONO} + \text{NO}_2$  and  $\text{NO}_2$ , respectively were measured. Immediately after the cell, the HONO flow was diluted into a few standard liters per minute stream of He before being introduced to the CIMS. The final mixing ratios of HONO ranged between 0.1 and 10 ppb (at 760 Torr). The second method involved the reaction between gaseous hydrogen chloride and solid sodium nitrite, as previously described by Aubin and Abbatt.<sup>16</sup> HCl from a permeation tube (VICI Metronics) maintained at 40 °C was carried by a flow of 200 sccm He into a PFA Teflon column packed with  $\text{NaNO}_2$ , where HONO was formed. The CIMS measurement showed that HONO produced by this method was  $\text{NO}_2$ -free, hence heterogeneous conversion of HONO to NO and  $\text{NO}_2$  on the  $\text{NaNO}_2$  and tubing wall surfaces was negligible.<sup>16</sup> The concentration of HONO was quantified by a  $\text{NO}_x$  monitor (Thermo Scientific). To determine the  $k_2/k_1$  ratio,  $\text{NO}_2$  was added to the flow reactor from a bulb along with HONO as described above. HONO

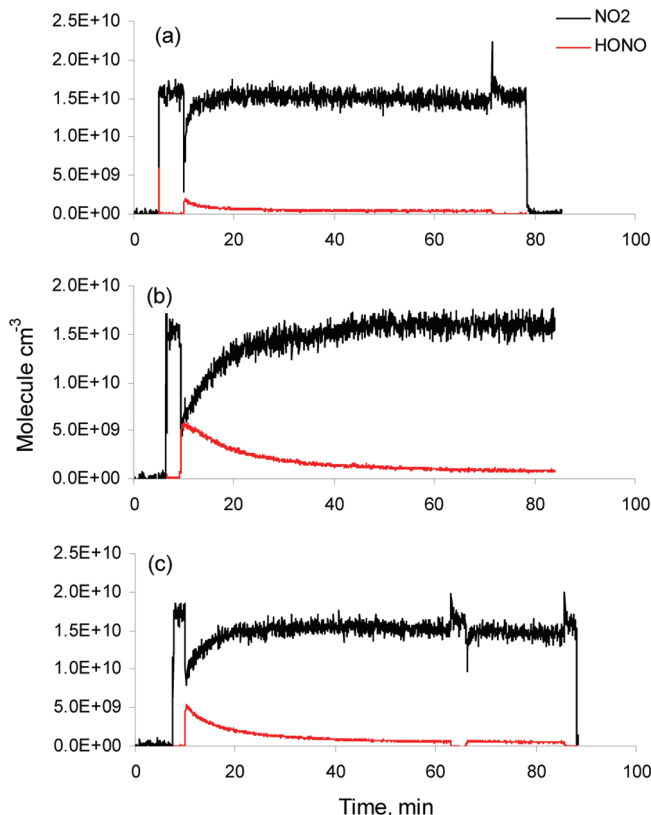


**Figure 2.** Uptake of  $\text{NO}_2$  and release of HONO on type B soot samples prepared using propane flame: (a) 1.9 mg of fresh soot; (b) 1.9 mg of preheated soot; (c) 1.2 mg of fresh soot extracted by *iso*-propanol.

calibrations produced by two independent methods agreed within  $\pm 15\%$ , resulting in a  $k_2/k_1$  ratio of 9.6, which was a factor of 2.2 higher than the value based on previous measurements.<sup>17</sup>

### 3. Results and Discussion

**3.1.  $\text{NO}_2$  Uptake and HONO Formation on Different Types of Soot.** Figure 2a presents temporal profiles for  $\text{NO}_2$  uptake and HONO formation on fresh type B propane soot. The initial drop of  $\text{NO}_2$  signal at 10 min corresponds to retracting the injector by 8 cm, thus exposing an 8 cm length of the soot film to  $\text{NO}_2$ . The initial rapid uptake of  $\text{NO}_2$  is followed by a slow asymptotic recovery, but complete saturation of the soot sample does not occur, and even after long exposure the  $\text{NO}_2$  signal remains below its initial level. When  $\text{NO}_2$  partitions to the surface, a simultaneous increase in the HONO signal is observed. The concentration of HONO reaches a maximum and then decreases exponentially and remains at a constant nonzero level. When  $\text{NO}_2$  exposure is terminated by moving the injector downstream the soot sample, the concentration of HONO drops to zero almost instantaneously, whereas  $\text{NO}_2$  signal peaks and then returns to the initial level. This intermittent rise corresponds

**TABLE 1: Number of NO<sub>2</sub> Molecules Taken and HONO Molecules Released for Fresh, Pre-Heated, and Extracted Type B Propane Flame Soot Samples**

soot sample	NO <sub>2</sub> × 10 <sup>-15</sup> , molecules mg <sup>-1</sup>	HONO × 10 <sup>-15</sup> , molecules mg <sup>-1</sup>
fresh	2.5 ± 0.9	1.1 ± 0.2
preheated to 300 °C	9.0 ± 0.9	7.2 ± 0.2
extracted by <i>iso</i> -propanol	6.3 ± 0.9	4.7 ± 0.2
extracted by toluene	2.0 ± 0.9	0.8 ± 0.2

to a release of NO<sub>2</sub> that is physically adsorbed on the soot surface. The observed variation in NO<sub>2</sub> signal, showing a fast reversible and a slow irreversible uptake, is in agreement with the heterogeneous mechanism that involves physical adsorption of NO<sub>2</sub> followed by chemical conversion to HONO through the reaction with reductive sites, for example, hydride, in an otherwise mostly elemental carbon backbone.<sup>9–12</sup> The fast decrease in the NO<sub>2</sub> uptake and HONO formation rates in the first few minutes of exposure, as displayed in Figure 2, have been previously explained by a temporary depletion of the surface adsorption sites.<sup>12</sup> Subsequent slow conversion of NO<sub>2</sub> to HONO may occur for hours. We used the area between recovery and steady state signals of NO<sub>2</sub> and the area under the signal of HONO to calculate the total number of NO<sub>2</sub> molecules irreversibly reacted on soot and HONO molecules produced, respectively. During the 70 min exposure period, 2.5 × 10<sup>15</sup> NO<sub>2</sub> molecules are consumed, whereas 1.1 × 10<sup>15</sup> HONO molecules are formed per 1 mg of fresh soot (Table 1). The instantaneous HONO yield, defined as [HONO]/(Δ[NO<sub>2</sub>]), remains fairly constant during reaction to the point where the NO<sub>2</sub> signal recovers to about 85% of its initial value. Note that this HONO yield (about 44%) was among the smallest yields for fresh soot samples observed in our study.

Preheating the soot sample to 300 °C in vacuum before the uptake experiment drastically increases its reactivity, as indicated by a larger drop in the NO<sub>2</sub> signal and larger increase in the HONO signal upon retracting the injector (Figure 2b). The number of NO<sub>2</sub> molecules reacted and HONO molecules formed are higher than those of unheated soot, by a factor of 3.6 and 6.5, respectively (Table 1). Incomplete combustion of hydrocarbon fuels produces a broad range of semivolatile organic products, such as polycyclic aromatic hydrocarbons (PAH), saturated and unsaturated hydrocarbons, and partially oxidized organics (e.g., alcohols, carbonyls, organic acids), which can condense on soot upon cooling.<sup>37,38</sup> Apparently, the increased reactivity of heated soot is caused by removal of incomplete combustion products, rendering more adsorptive and/or reactive surface sites. The presence of condensed material on the soot surface is indirectly confirmed by observing a thin organic film that builds up over time on the cool top part of the vacuum container used to heat soot-coated Pyrex tubes. The film is the thickest for kerosene soot and barely observable for propane soot samples, indicating that kerosene soot contains a larger organic fraction. Individual samples do not show a detectable decrease in their mass after heating, which indicates that even for kerosene soot the mass fraction of condensed organic material is less than 2%. Also, heating caused no visible changes in the infrared spectra of soot.

To examine the nature of condensed organic materials and their role on soot reactivity, we have investigated soot samples that were extracted by *iso*-propanol and toluene, which are expected to remove polar and nonpolar organics from the soot backbone, respectively. As shown in Figure 2c, soot samples treated by *iso*-propanol consume more NO<sub>2</sub> and form more HONO than the fresh soot for a similar exposure time, although

**TABLE 2: HONO Formation from Heterogeneous Reaction of NO<sub>2</sub> on Different Types of Soot<sup>a</sup>**

fuel	HONO × 10 <sup>-15</sup> , molecules mg <sup>-1</sup>			
	type A		type B	
	fresh	heated	fresh	heated
propane	1.5 ± 0.2	5.4 ± 0.2	0.8 ± 0.2	7.6 ± 0.2
	(58 ± 21)	(74 ± 11)	(38 ± 12)	(72 ± 9)
kerosene	2.5 ± 0.2	3.8 ± 0.2	0.8 ± 0.4	7.8 ± 0.2
	(86 ± 19)	(85 ± 10)	(53 ± 21)	(91 ± 8)

<sup>a</sup> HONO yields (%) are given in parentheses; sample mass is 1–4 mg.

**TABLE 3: BET Specific Surface Areas of Type A and Type B Propane and Kerosene Soot Samples<sup>a,b</sup>**

fuel	BET specific surface area, m <sup>2</sup> g <sup>-1</sup>	
	type A	type B
propane	79	147
kerosene	67 (61)	106 (116)

<sup>a</sup> Determined in our previous study;<sup>25</sup> before measurement, samples were preheated to 200 °C for 1 h. Values in parentheses are obtained in the present work. <sup>b</sup> Geometric surface area of the sample tube is 50.3 cm<sup>2</sup>.

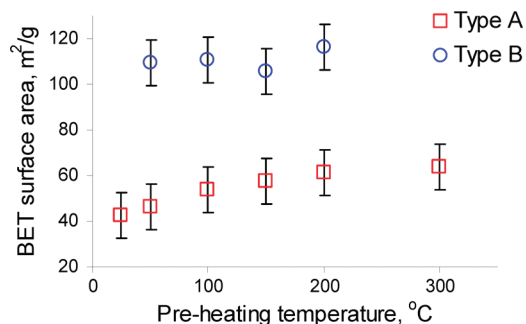
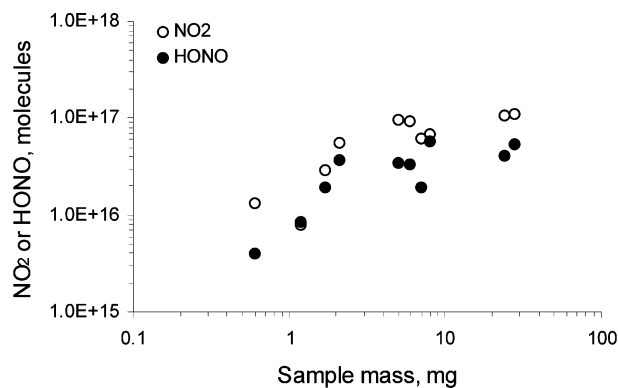
the enhancement in reactivity is not as pronounced as in the case of preheated soot. On the contrary, extraction of soot by toluene has no effect on the number of NO<sub>2</sub> molecules reacted or HONO molecules formed (Table 1). On the basis of the results of heating experiments, we conclude that most of adsorptive and reactive sites in our samples belong to the soot backbone rather than condensed organic material. Also, extraction experiments provide tentative evidence that molecules blocking these sites are of polar nature.

The amount of organic material on soot and its oxidation state depend on the flame equivalence ratio<sup>37</sup> (actual fuel to oxidizer ratio over the fuel to oxidizer ratio at stoichiometric conditions) and sample preparation method.<sup>12</sup> Soot particles are chain-like aggregates of elemental carbon spheres that are clearly identifiable in the soot produced under fuel-lean conditions,<sup>18</sup> but they appear blended and with less clear boundaries due to organic material in the case of a fuel-rich diffusion flame.<sup>26</sup> For the diffusion flame used in the present study, the fraction of organic carbon increases with the C/H ratio of the hydrocarbon fuel; also, it is higher for type A soot samples that are prepared by allowing the reducing part of the flame to touch the soot surface. Table 2 shows that the total amount of HONO formed upon heterogeneous interaction of NO<sub>2</sub> with soot depends on the fuel and sample preparation method. Among unheated samples, type A soot produces the highest amount of HONO, particularly when kerosene is used to generate soot films, whereas type B soot produces the least amount of HONO. After heating, however, the largest HONO production is observed for type B soot. Although fresh type A soot is already exposed to heat from the flame during preparation, this soot is not the same as preheated type B soot, because of the differences in their visual appearance, HONO formation capacity (Table 2), BET surface area (Table 3), and reactivity (Table 4).

A factor of 6.5–9.6 increase in the amount of HONO formed on heated type B soot cannot be explained merely from increased BET surface area, because the latter remains unchanged after heating (Figure 3). Since soot is a highly porous material, an important implication of the unchanged internal surface area is that the condensed material does not block pore throats. The internal surface area of soot samples calculated from

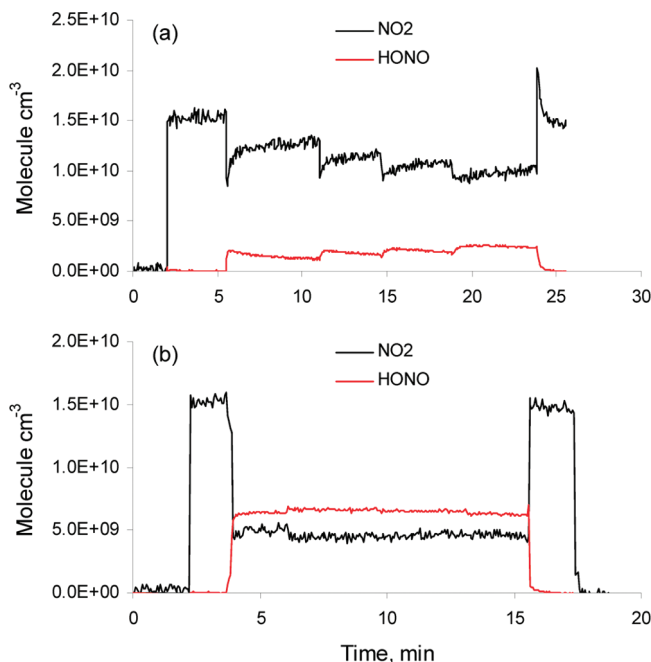
**TABLE 4: Irreversible Uptake Coefficients of NO<sub>2</sub> on Soot Calculated Using BET Surface Areas of Samples<sup>a</sup>**

fuel	uptake coefficient, $\gamma_{\text{BET}} \times 10^5$			
	type A		type B	
	fresh	heated	fresh	heated
propane	4.9 ± 3.0	23.0 ± 7.0	1.0 ± 0.7	4.3 ± 1.5
kerosene	1.6 ± 0.5	4.7 ± 1.4	1.6 ± 0.6	4.6 ± 1.7

<sup>a</sup> Sample mass is 1–7 mg.**Figure 3.** Dependence of the measured BET internal surface area of type A (6 mg) and type B (9 mg) kerosene flame soot on the sample preheating temperature.**Figure 4.** The integral number of NO<sub>2</sub> molecules taken and HONO molecules released by preheated type B propane soot samples of different mass.

BET isotherms is 2 orders of magnitude larger than their geometric surface (Table 3). To determine the actual surface area involved in the reaction with NO<sub>2</sub>, a series of uptake experiments were performed using soot samples of varied mass. Figure 4 shows that the number of NO<sub>2</sub> molecules consumed and HONO molecules released increase linearly with the soot sample mass initially, but level off for samples in excess of about 4 mg, which corresponds to a 0.1 mg cm<sup>-2</sup> critical surface density, in close agreement with the values measured in previous studies.<sup>10,13</sup> Even for soot samples with mass below 4 mg, total HONO production of (0.1–0.8) × 10<sup>16</sup> molecule mg<sup>-1</sup> is at the lower range of previously reported data, (1–4) × 10<sup>16</sup> molecule mg<sup>-1</sup>.<sup>10,12,14</sup> This can be attributable to that NO<sub>2</sub> is unable to reach deeper layers of soot on the time scale of our experiments and hence not all of internal surface areas of soot films are available for the heterogeneous reaction because of low NO<sub>2</sub> concentrations used in our study.

**3.2. Kinetics of NO<sub>2</sub> Uptake.** Measurements of the uptake coefficient were performed by exposing varying lengths of the soot film to NO<sub>2</sub> while monitoring the change in NO<sub>2</sub> and HONO signals. Unheated soot samples display a combination of reversible and irreversible uptakes (Figure 5a). Stepwise retracting of the injector leads to an uptake pattern with

**Figure 5.** Uptake of NO<sub>2</sub> and release of HONO on 16 mg type A propane flame soot: (a) fresh soot sample; (b) preheated soot sample.

progressively lower asymptotic NO<sub>2</sub> signal and less distinct reversible part at longer reaction times. The uptake of NO<sub>2</sub> on heated samples consists of irreversible part only and leads to higher HONO production (Figure 5b). A 50–70% drop in the NO<sub>2</sub> signal and a corresponding increase in the HONO signal are observed upon retracting the injector by 2 cm; however, little additional NO<sub>2</sub> uptake or HONO formation occurs when the exposed soot area is increased by further retracting the injector. This behavior indicates that gas-phase diffusion of NO<sub>2</sub> toward the sample surface and possibly inside the sample pores limit the rate of heterogeneous uptake on preheated soot. Furthermore, when the exposure is stopped by returning the injector to its initial position, little NO<sub>2</sub> is released by soot because all physically adsorbed nitrogen dioxide molecules have been converted to HONO or other species. Thus, whereas for unheated soot the overall uptake rate is limited by the number of vacant adsorptive and reactive sites, for heated samples diffusion and physical adsorption correspond to the limiting steps.

The asymptotic portions of the uptake curves at different injector positions were used to calculate the first-order loss constants,  $k_{\text{obs}}$ , by plotting the logarithm of NO<sub>2</sub> signal versus the soot-NO<sub>2</sub> interaction time (Figure 6). Note that  $k_{\text{obs}}$  corresponds to the irreversible reactive uptake and does not include the fast initial physical uptake. For the majority of experiments with preheated soot, only two points could be used in the regression analysis because no additional NO<sub>2</sub> loss was observed after retracting the injector beyond 2 cm length of the soot film. In such cases the observed loss constants and corresponding uptake coefficients derived for preheated soot samples represent a lower limit to actual values. The wall-loss rate constant,  $k_w$ , was calculated from the observed first-order loss by taking into account the diffusion of NO<sub>2</sub> in helium from the center of the reactor to the wall (eqs 3 and 4):<sup>39–41</sup>

$$\frac{1}{k_{\text{obs}}} = \frac{1}{k_d} + \frac{1}{k_w} \quad (3)$$

$$k_d = \frac{3.66 D_{P,He}}{r^2 P_{He}} \quad (4)$$

where  $D_{P,He}$  is the diffusion coefficient of NO<sub>2</sub> in helium at pressure  $P_{He}$  and  $r$  is the radius of the soot coated tube. Figure 7 shows that initially  $k_w$  increases with the sample mass, but levels off for samples in excess of 5–10 mg, in close agreement with the mass dependence observed for the total number of NO<sub>2</sub> molecules reacted on soot.

Large variability between measurements conducted for different soot samples may originate from variation in soot film properties, such as different amount of semivolatile materials generated by flame or nonuniformity in the soot film thickness along the tube length. Control experiments show good reproducibility for consecutive measurements carried out using the same soot sample. For each repetitive exposure, the NO<sub>2</sub> loss rate decreases by less than 5–10%. Hence, only a small fraction of soot reactive sites are consumed in kinetic experiments carried out over short time scale using low NO<sub>2</sub> concentrations ( $1-2 \times 10^{10}$  molecules cm<sup>-3</sup>). Use of longer exposure times or higher

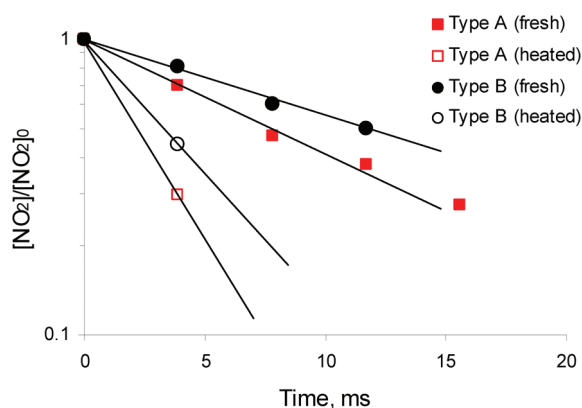


**Figure 6.** Kinetics of NO<sub>2</sub> loss on different types of propane flame soot (type A and B soot sample mass is 8 and 7 mg, respectively).

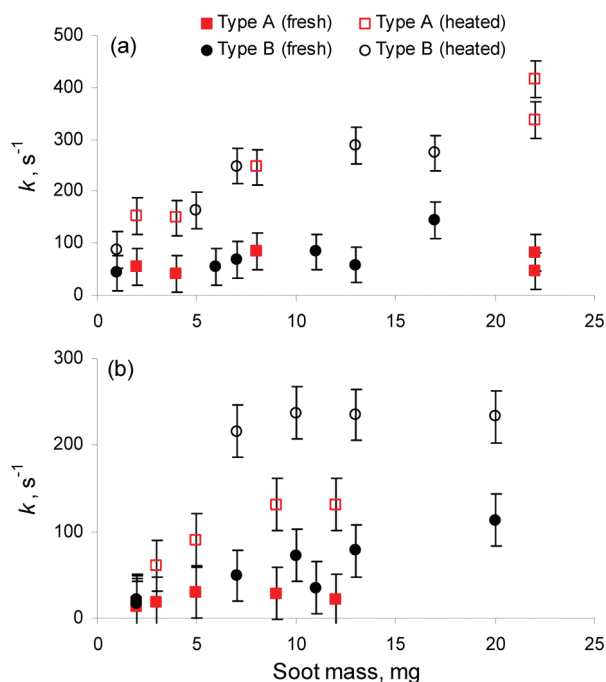


**Figure 7.** Dependence of the NO<sub>2</sub> loss rate on the soot sample mass: (a) propane flame soot; (b) kerosene flame soot. For all data the sample mass corresponds to a 10 cm length of the soot coating.

NO<sub>2</sub> concentrations (ca.  $5 \times 10^{11}$  molecules cm<sup>-3</sup>) results in gradual deactivation of soot samples on a time scale of a single kinetic experiment. Also, the reactivity of soot samples that are exposed to ambient air for several days is reduced by more than 1 order of magnitude.

NO<sub>2</sub> uptake coefficients,  $\gamma_{BET}$ , were calculated according to eq 5 using internal surface areas of soot films,  $A_{BET}$ , obtained from BET measurements (Table 3):

$$\gamma_{BET} = \frac{2k_w V}{\omega A_{geom}} = \frac{2rk_w A_{geom}}{\omega A_{BET}} \quad (5)$$

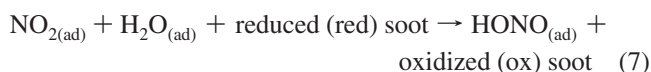
where  $\omega$  is the mean molecular speed of NO<sub>2</sub> and  $A_{geom}$  is geometric surface area of the sample. The results are summarized in Table 4, which presents values of  $\gamma_{BET}$  averaged over several soot samples with masses in the range 1–7 mg. Fresh soot has the lowest reactivity,  $\gamma_{BET} = (1-5) \times 10^{-5}$ , which increases by a factor of 3–5 after preheating of the samples in vacuum to 300 °C. The effect of heating may explain the variation in the reactivity and HONO production capacity of soot samples. Our kinetic data are in good agreement with previously reported NO<sub>2</sub> uptake coefficients ( $\gamma_{BET} = 10^{-6}$  to  $10^{-4}$ ) that were derived using BET surface areas.<sup>16</sup>

### 3.3. Mechanism of NO<sub>2</sub> Uptake and HONO Formation.

Observation of HONO yields in excess of 50% and absence of HNO<sub>3</sub> among the reaction products unambiguously rule out the surface-catalyzed disproportionation of NO<sub>2</sub> in water as a major pathway for HONO formation (reaction 6):

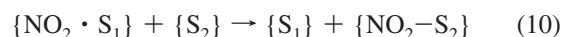
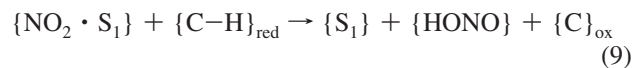


Pumping on the soot samples for extended period of time to remove adsorbed water has no effect on the HONO yield, indicating that water is not involved in the redox reaction of NO<sub>2</sub> with soot active sites (reaction 7),<sup>10</sup>



Also, we observed no reactivation of the NO<sub>2</sub>-processed soot samples after exposure to elevated relative humidity.

Our results support a mechanism in which the soot surface itself provides a hydrogen atom for NO<sub>2</sub> to form HONO.<sup>10,12,16</sup> Initial uptake of NO<sub>2</sub> occurs through physical adsorption (reaction 8) and corresponds to the reversible part of curves shown in Figures 2 and 5a (brackets denote adsorbed species and surface sites).



HONO is formed through chemical interaction of the adsorbed NO<sub>2</sub> with reducing surface sites,  $\{C-H\}_{red}$ , such as allylic

hydrogens (reaction 9).<sup>16,42</sup> Soot acts as a consumable reactant rather than a catalyst and cannot be recycled. Reaction 10 has been previously invoked to explain formation of nitrogen-containing species on the soot surface in experiments with high ( $\sim 10$  ppm)  $\text{NO}_2$  concentrations.<sup>11</sup> However, its contribution is expected to be negligible under low  $\text{NO}_2$  conditions ( $\sim 1$  part per billion) of our experiments.<sup>12,16</sup>

The fast initial decrease in the  $\text{NO}_2$  uptake rate on fresh soot is caused by depletion of surface adsorption sites  $\{S_1\}$ . The rate of subsequent irreversible reaction involving adsorbed  $\text{NO}_2$  is limited by the availability of  $\{C-H\}_{\text{red}}$  reactive sites, a large fraction of which are blocked by condensed organic material. Heating the soot film removes the organics that blocks these reactive sites, resulting in an increased irreversible uptake rate. This may explain the apparent partial reactivation of  $\text{NO}_2$ -processed soot by heating reported previously.<sup>10</sup> Heated and extracted soot films that have been depleted of reactive sites show no enhancement in the  $\text{NO}_2$  desorption peak relative to that for fresh soot (Figure 2). The absence of increased physical adsorption indicates that organic molecules from incomplete combustion and  $\text{NO}_2$  occupy different adsorptive sites on the soot surface. The same is true for adsorption of Kr atoms because removal of organic material by heating the soot film has little or no effect on the internal surface area derived from BET adsorption isotherms measured using Kr (Figure 3).

According to the redox mechanism outlined above, the oxidation state of soot surface largely determines the reactivity of soot toward  $\text{NO}_2$ . Less oxidized (type A) and preheated soot films react at a faster rate and form larger absolute amounts of HONO at higher relative HONO yields, which approach 90% (Table 2). Lower HONO yields on oxidized (type B) soot can be caused by reaction of HONO with polar organic compounds adsorbed on soot surface. This is in agreement with previous studies by Rossi and co-workers who suggested that  $\text{NO}_2$  is converted to HONO at a 100% yield on any soot, but some of the HONO may react on the surface to form NO (eq 12).<sup>12,13</sup> Future research is required to identify the nature of the polar species converting HONO to NO. Possible candidates are hydroxylated PAH,<sup>38,43</sup> such as phenols and alkyl aryl alcohols, which can be oxidized by HONO to benzoquinonoxims<sup>44</sup> and alkyl aryl carbonyls.<sup>45</sup>

### 3.4. $\text{NO}_2$ Uptake and HONO Formation on Coated Soot.

Our study provides experimental evidence that condensed materials have a significant impact on heterogeneous interaction between  $\text{NO}_2$  and soot. To further investigate the effect of coatings, we examined  $\text{NO}_2$  uptake on soot films that were pretreated with vapors of pyrene, sulfuric acid, and glutaric acid. Although no measurable increase in the sample mass was observed after coating (i.e., less than 2% or  $10^{17}$  molecules  $\text{mg}^{-1}$ ), the presence of the coating materials on soot was confirmed from ATR-FTIR spectra as shown in Figure 8. Spectra taken at different locations along the tube (top, middle, and bottom) show that a thicker coating is deposited on the bottom part that faces the coating material whereas the top and middle parts are coated uniformly. Therefore, uptake experiments were performed by exposing only the top and middle parts of the tubes to  $\text{NO}_2$ . Control runs indicate that  $\text{NO}_2$  does not react with pure coating materials in the absence of soot under conditions of our experiments. Figure 9 shows that  $\text{NO}_2$  uptake and HONO production vary greatly depending on the nature of the coating material. Uptake coefficients, total numbers of  $\text{NO}_2$  molecules reacted and HONO molecules formed, and relative HONO yields measured for coated soot samples are summarized in Tables 5 and 6.

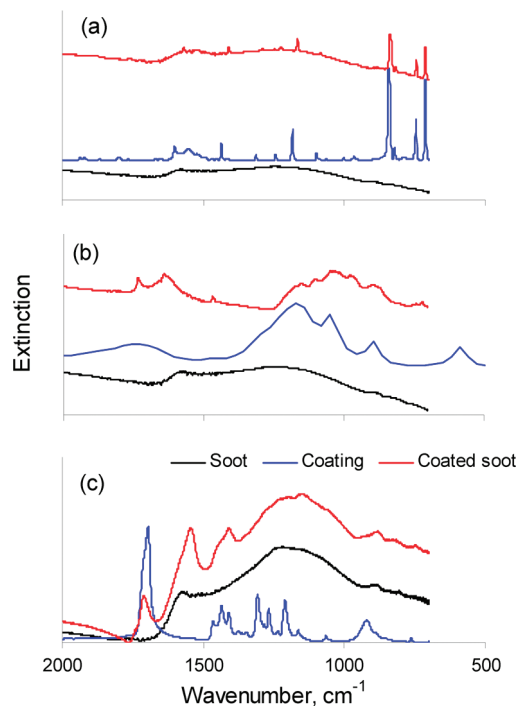


**Figure 8.** ATR-FTIR extinction spectra of type B kerosene flame soot before and after exposure to vapor of (a) pyrene, (b) sulfuric acid, and (c) glutaric acid. Spectra of pure coating materials are given for reference.

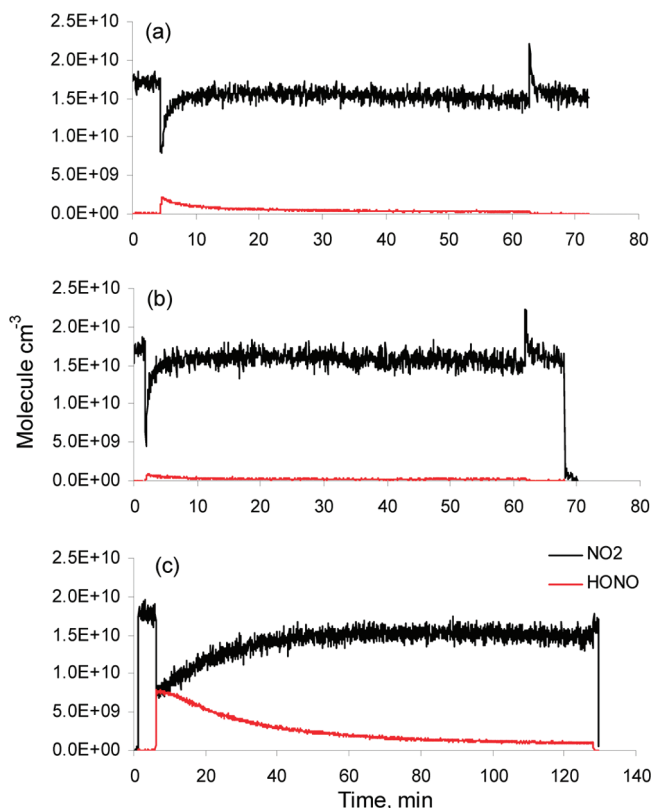


**Figure 9.** Uptake of  $\text{NO}_2$  and formation of HONO on type B propane soot coated by different materials: (a) pyrene, soot mass 1.6 mg; (b) sulfuric acid, soot mass 3.5 mg; (c) glutaric acid, soot mass 1.2 mg.

Experiments with soot coated by pyrene show no significant change in the uptake rate (Table 5), HONO yield (Table 6), or amount of  $\text{NO}_2$  desorbed after exposure (Figure 9b), indicating that pyrene blocks neither adsorptive nor reactive surface sites. Pyrene belongs to a class of polycyclic aromatic hydrocarbons

**TABLE 5: Irreversible Uptake Coefficients of NO<sub>2</sub> on Coated Type B Soot and Corresponding HONO Yields<sup>a</sup>**

coating	uptake coefficient, $\gamma_{\text{BET}} \times 10^5$	
	propane	kerosene
pyrene	1.5 ± 0.7	1.7 ± 0.3
sulfuric acid	1.4 ± 0.4	2.0 ± 0.8
glutaric acid	4.2 ± 1.4	3.0 ± 1.3

<sup>a</sup> Uptake coefficients were calculated using BET surface areas of soot samples; sample mass is 1–7 mg.

**TABLE 6: Number of NO<sub>2</sub> Molecules Taken, HONO Molecules Released, and Corresponding HONO Yields for Coated Type B Propane Flame Soot Samples<sup>a</sup>**

coating	NO <sub>2</sub> × 10 <sup>-15</sup> , molecules mg <sup>-1</sup>	HONO × 10 <sup>-15</sup> , molecules mg <sup>-1</sup>	HONO yield %
pyrene	1.9 ± 0.9	1.3 ± 0.2	68 ± 18
sulfuric acid	0.8 ± 0.9	0.3 ± 0.2	38 ± 34
glutaric acid	20.2 ± 0.9	17.3 ± 0.2	86 ± 5

<sup>a</sup> Sample mass is 1–7 mg.

(PAH) produced from incomplete combustion. Our measurements imply that although PAH may contribute a significant fraction of the organic soot mass, particularly for soot formed in fuel-rich flames,<sup>46</sup> their effect on the soot reactivity toward NO<sub>2</sub> is negligible.

The presence of sulfuric acid coating on soot has little effect on the NO<sub>2</sub> uptake coefficient, but significantly reduces the absolute amount of released HONO. Since sulfuric acid is less reactive toward NO<sub>2</sub> than soot ( $\gamma < 10^{-6}$  has been reported for surfaces of H<sub>2</sub>SO<sub>4</sub> solutions<sup>47</sup>), an unchanged uptake coefficient on the H<sub>2</sub>SO<sub>4</sub>-coated surface indicates that sulfuric acid does not impede the interaction between NO<sub>2</sub> and soot. The observed low production of HONO can be explained by acid-catalyzed conversion of {HONO} to NO. Our results are consistent with those reported earlier for commercial carbon samples coated by H<sub>2</sub>SO<sub>4</sub>, where the HONO yield decreased to nearly zero and the yield of NO increased with increasing sulfuric acid surface coverage.<sup>11</sup> After cycling of the coated soot sample through elevated relative humidity (i.e., humidification to 100% RH followed by drying), the absolute amount of HONO formed in the reaction decreases to zero, but the NO<sub>2</sub> uptake coefficient remains virtually unchanged. Upon humidification, sulfuric acid absorbs water, increasing the coating volume by more than an order of magnitude.<sup>48</sup> When humidity is decreased, water evaporates and leaves behind a thin film of sulfuric acid evenly distributed on the soot surface, making H<sub>2</sub>SO<sub>4</sub> readily available for interaction with {HONO}. Preheating H<sub>2</sub>SO<sub>4</sub>-coated soot samples to 200 °C partially restores the HONO production, but does not change the uptake coefficient. Incomplete recovery of HONO production can be caused by sulfuric acid remaining in the soot pores or by sulfuric acid-induced oxidation of the soot surface during heating.

Coating the soot films by glutaric acid increases the NO<sub>2</sub> uptake rate and the amount of formed HONO by a factor of 2–4 and 20–25, respectively. The magnitude of this enhancement is comparable to or even exceeds that observed for preheated soot. It is notable that absolute and relative HONO yields are both increased after coating (Table 6), which indicates that either more HONO is produced for each consumed NO<sub>2</sub> molecule or less HONO is converted to NO on the soot surface. We hypothesize that glutaric acid forms strong hydrogen-bonded complexes<sup>49</sup> with polar organic molecules from the flame occupying {C–H}<sub>red</sub> sites on the soot surface. Binding those polar molecules to glutaric acid not only makes the reactive

sites accessible to NO<sub>2</sub>, but also reduces conversion of adsorbed HONO to NO through reaction 12. Similarly to pyrene and sulfuric acid, glutaric acid does not change the number of vacant adsorption sites {S<sub>1</sub>} because reversible NO<sub>2</sub> uptake and internal BET surface area of soot remain unaffected by coating.

#### 4. Conclusions

We have used a fast-flow reactor to study heterogeneous reaction of nitrogen dioxide with hydrocarbon soot produced under rich (type A) and lean (type B) combustion conditions. The irreversible uptake coefficient and HONO yield are the highest for less oxidized type A soot. Heating of the soot samples in vacuum removes condensed organic materials and unblocks reactive sites, leading to increased uptake coefficients and HONO yields. A comparable enhancement is also observed after extracting the soot samples with *iso*-propanol, which indicates that organic molecules blocking reactive sites have polar nature. The impact of condensed materials is further investigated using soot films pretreated with vapors of pyrene, sulfuric acid, or glutaric acid. Coating of pyrene has little effect on either reaction rate or HONO yield. Sulfuric acid coating does not alter the uptake coefficient, but significantly reduces the amount of HONO formed. Coating of glutaric acid significantly increases NO<sub>2</sub> uptake coefficient and HONO yield. These results imply that the reactivity and HONO generating capacity of internally mixed soot aerosol will be strongly dependent on the chemical composition of the coating material and hence will vary greatly in different polluted environments.

Irreversible uptake coefficients of NO<sub>2</sub> on fresh soot calculated using BET surface areas of samples have the initial values of (1–5) × 10<sup>-5</sup>. Hence, from a kinetic perspective (eq 13), about 1 ppb of HONO can be produced during night for typical NO<sub>2</sub> concentrations and soot surface loadings ( $\sigma$ ) in the urban troposphere, assuming no deposition losses for HONO.<sup>9</sup>

$$\frac{d[\text{HONO}]}{dt} = \frac{\gamma\sigma\omega[\text{NO}_2]}{4} \quad (13)$$

However, continuous exposure to NO<sub>2</sub> reduces the reactivity of soot because of deactivation of the surface sites. Furthermore, soot particles will be coated with inorganic and organic species during their atmospheric aging,<sup>18</sup> which may enhance or reduce their reactivity with NO<sub>2</sub> and HONO formation.

**Acknowledgment.** This work was supported by the Houston Advanced Research Center (HI01), National Science Foundation (AGS-0938352 and CBET-0932705), and the Robert A. Welch Foundation (Grant A-1417). R. Z. acknowledges additional support from the National Natural Science Foundation of China Grant (40728006). We thank Sarah Brooks for the use of an analytical balance.

#### References and Notes

- (1) Febo, A.; Perrino, C.; Allegrini, I. *Atmos. Environ.* **1996**, *30*, 3599.
- (2) Winer, A. M.; Biermann, H. W. *Res. Chem. Intermed.* **1994**, *20*, 423.
- (3) Stutz, J.; Alicke, B.; Ackermann, R.; Geyer, A.; Wang, S. H.; White, A. B.; Williams, E. J.; Spicer, C. W.; Fast, J. D. *J. Geophys. Res.* **2004**, *109*, 14.
- (4) Lammel, G.; Cape, J. N. *Chem. Soc. Rev.* **1996**, *25*, 361.
- (5) Aumont, B.; Madronich, S.; Ammann, M.; Kalberer, M.; Baltensperger, U.; Hauglustaine, D.; Brocheton, F. *J. Geophys. Res.* **1999**, *104*, 1729.
- (6) Penner, J. E.; Eddleman, H.; Novakov, T. *Atmos. Environ., Part A* **1993**, *27A*, 1277.

- (7) IPCC Intergovernmental Panel on Climate Change. *Report*. Ed Solomon, S.; Cambridge Univ Press: Cambridge, UK, 2007; <http://www.ipcc.ch/ipccreports/ar4-wg1.htm>.
- (8) Lei, W. F.; Zhang, R. Y.; Tie, X. X.; Hess, P. *J. Geophys. Res.* **2004**, *109*, D12301.
- (9) Ammann, M.; Kalberer, M.; Jost, D. T.; Tobler, L.; Rossler, E.; Piguet, D.; Gaggeler, H. W.; Baltensperger, U. *Nature* **1998**, *395*, 157.
- (10) Gerecke, A.; Thielmann, A.; Gutzwiller, L.; Rossi, M. *J. Geophys. Res. Lett.* **1998**, *25*, 2453.
- (11) Kleffmann, J.; Becker, K. H.; Lackhoff, M.; Wiesen, P. *Phys. Chem. Chem. Phys.* **1999**, *24*, 5443.
- (12) Stadler, D.; Rossi, M. *J. Phys. Chem. Chem. Phys.* **2000**, *2*, 5420.
- (13) Salgado, M. S.; Rossi, M. *J. Int. J. Chem. Kinet.* **2002**, *34*, 620.
- (14) Lelievre, S.; Bedjanian, Y.; Laverdet, G.; Le Bras, G. *J. Phys. Chem. A* **2004**, *108*, 10807.
- (15) Kleffmann, J.; Wiesen, P. *Atmos. Chem. Phys.* **2005**, *5*, 77.
- (16) Aubin, D. G.; Abbatt, J. P. D. *J. Phys. Chem. A* **2007**, *111*, 6263.
- (17) Longfellow, C. A.; Ravishankara, A. R.; Hanson, D. R. *J. Geophys. Res.* **1999**, *104*, 13833.
- (18) Zhang, R.; Khalizov, A. F.; Pagels, J.; Zhang, D.; Xue, H.; McMurry, P. H. *Proc. Natl. Acad. Sci. U.S.A.* **2008**, *105*, 10291.
- (19) Shiraiwa, M.; Kondo, Y.; Moteki, N.; Takegawa, N.; Miyazaki, Y.; Blake, D. R. *Geophys. Res. Lett.* **2007**, *34*, L16803.
- (20) Fan, J.; Zhang, R. *Environ. Chem.* **2004**, *1*, 140.
- (21) Lei, W. F.; Zhang, R. Y.; McGivern, W. S.; Derecskei-Kovacs, A.; North, S. W. *Chem. Phys. Lett.* **2000**, *326*, 109.
- (22) Suh, I.; Lei, W. F.; Zhang, R. Y. *J. Phys. Chem. A* **2001**, *105*, 6471.
- (23) Saxena, P.; Hildemann, L. M. *J. Atmos. Chem.* **1996**, *24*, 57.
- (24) Aubin, D. G.; Abbatt, J. P. *Environ. Sci. Technol.* **2006**, *40*, 179.
- (25) Levitt, N. P.; Zhang, R. Y.; Xue, H. X.; Chen, J. M. *J. Phys. Chem. A* **2007**, *111*, 4804.
- (26) Zhang, D.; Zhang, R. *Environ. Sci. Technol.* **2005**, *39*, 5722.
- (27) Khalizov, A. F.; Zhang, R.; Zhang, D.; Xue, H.; Pagels, J.; McMurry, P. H. *J. Geophys. Res.* **2009**, *114*, D05208.
- (28) Khalizov, A. F.; Xue, H.; Wang, L.; Zheng, J.; Zhang, R. *J. Phys. Chem. A* **2009**, *113*, 1066.
- (29) Xue, H.; Khalizov, A. F.; Wang, L.; Zheng, J.; Zhang, R. *Environ. Sci. Technol.* **2009**, *43*, 2787.
- (30) Xue, H. X.; Khalizov, A. F.; Wang, L.; Zheng, J.; Zhang, R. Y. *Phys. Chem. Chem. Phys.* **2009**, *11*, 7869.
- (31) Aubin, D. G.; Abbatt, J. P. *J. Phys. Chem. A* **2003**, *107*, 11030.
- (32) McCabe, J.; Abbatt, J. P. D. *J. Phys. Chem. C* **2009**, *113*, 2120.
- (33) Brunauer, S.; Emmett, P. H.; Teller, E. *J. Am. Chem. Soc.* **1938**, *60*, 309.
- (34) Yanazawa, H.; Ohshika, K.; Matsuzawa, T. *Adsorpt—J. Int. Adsorpt. Soc.* **2000**, *6*, 73.
- (35) Zhang, R.; Leu, M. T.; Molina, M. J. *Geophys. Res. Lett.* **1996**, *23*, 1669.
- (36) Zhang, R. Y.; Leu, M. T.; Keyser, L. F. *J. Phys. Chem.* **1996**, *100*, 339.
- (37) Slowik, J. G.; Cross, E. S.; Han, J. H.; Kolucki, J.; Davidovits, P.; Williams, L. R.; Onasch, T. B.; Jayne, J. T.; Kolb, C. E.; Worsnop, D. R. *Aerosol Sci. Technol.* **2007**, *41*, 734.
- (38) Goldberg, E. D. *Black Carbon in the Environment: Properties and Distribution*; J. Wiley: New York, 1985.
- (39) Zhang, R.; Suh, I.; Lei, W.; Clinkenbeard, A. D.; North, S. W. *J. Geophys. Res.* **2000**, *105*, 24627.
- (40) Molina, M. J.; Molina, L. T.; Zhang, R. Y.; Meads, R. F.; Spencer, D. D. *Geophys. Res. Lett.* **1997**, *24*, 1619.
- (41) Zhang, R. Y.; Leu, M. T.; Keyser, L. F. *Geophys. Res. Lett.* **1995**, *22*, 1493.
- (42) Pryor, W. A.; Lightsey, J. W. *Science* **1981**, *214*, 435.
- (43) Smith, D. M.; Akhter, M. S.; Jassim, J. A.; Sergides, C. A.; Welch, W. F.; Chughtai, A. R. *Aerosol Sci. Technol.* **1989**, *10*, 311.
- (44) Adachi, A.; Okano, T. *Chemosphere* **2003**, *51*, 441.
- (45) Moodie, R. B.; Richards, S. N.; Thorne, M. P. *J. Chem. Soc.-Chem. Comm.* **1987**, 870.
- (46) Slowik, J. G.; Stainken, K.; Davidovits, P.; Williams, L. R.; Jayne, J. T.; Kolb, C. E.; Worsnop, D. R.; Rudich, Y.; DeCarlo, P. F.; Jimenez, J. L. *Aerosol Sci. Technol.* **2004**, *38*, 1206.
- (47) Kleffmann, J.; Becker, K. H.; Wiesen, P. *Atmos. Environ.* **1998**, *32*, 2721.
- (48) Tang, I. N. *J. Geophys. Res.* **1996**, *101*, 19245.
- (49) Zhao, J.; Khalizov, A.; Zhang, R.; McGraw, R. *J. Phys. Chem. A* **2009**, *113*, 680.